Optimal open loop wind farm control

Vitulli, J. A.; Larsen, Gunner Chr.; Pedersen, M. M.; Ott, Søren; Friis-Møller, Mikkel

Published in:
Proceedings of the Wake Conference 2019

Link to article, DOI:
10.1088/1742-6596/1256/1/012027

Publication date:
2019

Document Version
Publisher's PDF, also known as Version of record

Optimal open loop wind farm control

Optimal open loop wind farm control

J.A. Vitulli, G.C. Larsen, M.M. Pedersen, S. Ott and M. Friis-Møller

Technical University of Denmark, Department of Wind Energy
E-mail: gula@dtu.dk

Abstract. This paper presents a general purpose platform for optimal *open loop control* of wind power plants as seen from a power production perspective. The general idea is to change the controller design criteria from greedy individual wind turbines to a controller design facilitating cooperative and interdependent elements of a wind power plant, with the overall aim to improve the wind power plant power production conditioned on ambient mean wind speed and mean wind direction.
The flow within the wind power plant, including all essential interactions between the wind turbines, is modelled using a very fast linearized CFD RANS solver. The wind turbines are modelled as actuator discs, and two design variables per wind turbine - collective pitch, α, and tip speed ratio, λ - are initially defined for the optimization problem. However, a priory we expect one design variable to suffice - i.e. the unique set of (α, λ) representing the lowest thrust coefficient, C_T, for a given power coefficient C_p. The conjectured collapse of the design space is justified in this paper.
Optimized control schemes for the Lillgrund offshore wind farm are derived conditioned on ambient mean wind direction and wind speed. Aggregated over a year, using the site sector Weibull distributions, an increase in the annual energy production of 1% is demonstrated.

1. Introduction

Cost of energy (COE) is the most important single factor for the development of renewables in the energy system. Reduction of COE is, among other things, directly related to operational control of Wind Power Plants (WPP) as a whole as well as the individual wind turbines (WT) within them.
The aim of the present paper is to describe a recently developed general purpose platform for optimal *open loop control* of WPP's as seen from a power production perspective taking a WT de-rating approach. The general idea is to change the controller design criteria from "greedy" individual WT's to a controller design facilitating cooperative and interdependent behaviour of the WPP WT's for mutual benefit.

The WPP flow, including all essential interactions between the WPP WT's, is modelled using the linearized CFD RANS solver Fuga [1]. Fuga is taking advantage of the linearization to formulate the solution of the Navier Stokes equations in a mixed spectral domain, whereby the computational speed is reduced to a fraction of what is characteristic for traditional RANS solvers. This feature makes Fuga ideally suited as "working horse" in an optimization context.

The WT's are modelled as actuator discs, and two design variables per WT - collective pitch, α, and tip speed ratio, λ - are initially defined for the optimization problem. However, a priory we expect one design variable to suffice - i.e. the unique set of (α, λ) representing the lowest thrust coefficient, C_T, for a given power coefficient C_p different from maximum C_p. The conjectured collapse of the design space is justified in the paper.

For the optimization approach, we use a re-vitalized version of the WPP topology optimization platform TOPFARM [2], [3], with the objective function restricted to power production, and with the

original two WT position coordinates spanning the design space replaced by WT design sets (α_i, λ_i), where "*i*" refers to the *i*'th WT. The actuator discs defined for the Fuga WPP flow field modelling are based on power- and thrust coefficients, $C_p(U|\alpha,\lambda)$ and $C_t(U|\alpha,\lambda)$, both conditioned on (α, λ), and with U denoting the mean wind speed. In the optimization loop, $C_p(U|\alpha,\lambda)$ and $C_t(U|\alpha,\lambda)$ are obtained from surrogate models based on full aerodynamic simulations of the WT rotors assuming *stiff blades and tower* which, however, can be relaxed to fully flexible rotors if requested.

The control platform offers optimized WPP control schemes, conditioned on ambient mean wind speed and mean wind direction (i.e. essentially the WPP layout topology).

This is not the first attempt to develop such optimized open loop control strategies, as others have also conducted works on this innovative topic. An optimized *pitch-based* control strategy was examined in [4] yielding an annual energy production (AEP) gain of 0.33 % on the Princess Amalia Wind farm. Proposing a methodology that considered optimizing only the *pitch setting* of each turbine by using a genetic algorithm (GA) to navigate through the design space, it was shown in [5] that proper pitch angle selection could in fact improve overall farm performance. Furthermore, based off the work of Lee [5], an optimization procedure founded on a two-parameter design space for a given wind speed and wind direction was further developed in [6] that improved the global AEP by 1.56 % when applied onto an 80-WT wind farm in a rectangular grid arrangement compared to normal operation settings (variable speed configuration). All previous studies are based on simple engineering wake models, and most of these operate with only one design variable per WT. An exception is [6], which operates with the same two design parameters per WT as used in the present study. However, contrary to the this study, the present study is based on a *consistent CFD based flow model* to resolve the complex wind field inside a WPP, and further a consistent collapse of the two-parameter design space to a one-parameter design space per WT is introduced for improved computational performance.

The paper is structured as follows: First the platform is described in some detail in Section 2; then follows in Section 3 a sanity check of the platform performance. Section 4 describe and justify a collapse of the WPP control design space from two to one design parameters for each WT, which significantly increase the computational speed. The one-parameter tool is then used to develop sets of optimized control schedules for the Lillgrund offshore WPP in Section 5, and conclusions are finally drawn in Section 6.

2. The platform

The optimization platform consists of 4 key elements: 1) A flow model capable of describing the *steady flow* within a wind farm; 2) An aerodynamic model which, based on a detailed aerodynamic description of the rotor and its operational conditions (i.e. tip speed ratio and collective pitch setting), model the rotor power- and thrust, respectively; 3) A *fast* and accurate surrogate model of the detailed aerodynamic model; and 4) An optimization platform which, based on an objective function (i.e. WPP production) and selected WT specific constraints (i.e. upper and lower limits on α and λ), compute optimal WPP control schedules conditioned on the ambient inflow conditions (i.e. mean wind speed and mean wind direction).

A basic assumption is that *steady* flow modeling suffices when only *power production* is considered. This was investigated in [7], where production predictions from both Fuga and the medium-fidelity non-steady DWM model [8], [9], [10] were successfully compared to full-scale measurements.

2.1. The flow model

Computational *speed* is of crucial importance, since the WPP flow field needs to be re-computed in each iterative optimization step until convergence. Typically, the required number of iterations are of the range 200 - 1000 for a *specific* mean wind direction and mean wind speed, and this process then needs to be conducted for typically 10 mean wind speeds (mainly below rated wind speed) and 360 mean wind directions.

Fuga is a *linear* CFD RANS model ideally suited for this purpose. The governing Navier Stokes equations are consistently linearized and conveniently formulated in a *mixed spectral* domain, which

facilitates extremely fast solutions as based on a "system" of *look-up tables*, where some are general and some are WT specific. These tables are used to determine the velocity field behind a single solitary WT. Due to the linearity of the model, multiple wakes from many turbines can be constructed from the wake dictated velocity perturbation of a single turbine. These are in turn constructed from Fourier components by a fast Fourier integral transform.

The WT's are modelled as *actuator discs*, and the wind field conditions at each WT location inside the WPP will depend on wakes from neighboring upstream WT's. For a given wind direction the turbines locations are therefore first sorted according to their upwind distance, and subsequently the local wind speed, the thrust coefficient and the power production are evaluated starting with the undisturbed upwind turbines locations and progressively evaluating WT locations in the downwind direction. Finally, when the thrust of all turbines is known for the specified ambient wind conditions, we can evaluate the combined wake velocity deficit at any position – i.e. the complete WPP flow field. This process is handled by PyWake [11], an open source python framework for calculating AEP including wake effects. For more details, we refer to [1].

2.2. The WT aerodynamic model

For calculating the *aerodynamic* performance of the rotor, the linearized aeroservoelastic HAWCStab2 code [12] for steady state computation and stability analysis of WT's is used. The aerodynamic model in this code is based on a variant of the traditional BEM code [13], meaning that detailed aerodynamic description of the rotor is needed (i.e. blade twist and blade profiles with their respective aerodynamic coefficients). Although the code allows for fully flexible description of the WT main components, we have for our application assumed no elastic deformation of WT components, because such are not considered to influence the WPP flow field, the static WT thrust and the static WT production significantly. It is, however, straight forward to include equilibrium static WT deformations conditioned on the mean wind speed.

In the present framework, the WT's are represented by *uniformly loaded* actuator discs characterized by their individual power- and thrust coefficients (i.e. $C_p\,(U \mid \alpha, \lambda)$ and $C_t\,(U \mid \alpha, \lambda)$, respectively), conditioned on the WT operational conditions expressed in terms of the mean hub height wind speed, U, the collective pitch setting, α, and the tip speed ratio, λ, defined as (assuming zero yaw error)

$$\lambda \equiv \frac{R\Omega}{U} \tag{1}$$

where R denotes the rotor radius, and Ω is rotor rotational speed. The WT dimensionless power- and thrust coefficients are defined by respectively

$$C_p(U|\alpha,\lambda) \equiv \frac{P_{WT}(U|\alpha,\lambda)}{½\rho A U^3} \tag{2}$$

and

$$C_t(U|\alpha,\lambda) \equiv \frac{T_{WT}(U|\alpha,\lambda)}{½\rho A U^2} \tag{3}$$

in which ρ is the air density, P_{WT} denotes WT power production, and T_{WT} is the along wind rotor thrust force. The latter two result from the aerodynamic model. A is the rotor area and, accounting for both rotor tilt (θ_t) and rotor coning (θ_c), it may be expressed as

$$A = \pi(R\cos\theta_c\cos\theta_t)^2 \tag{4}$$

Using the HAWCStab2 code, example contour curves of respectively C_p and C_t surfaces are computed and shown as function of tip speed ratio and collective pitch in Figure 1 for a hub mean wind speed equal to 8m/s.

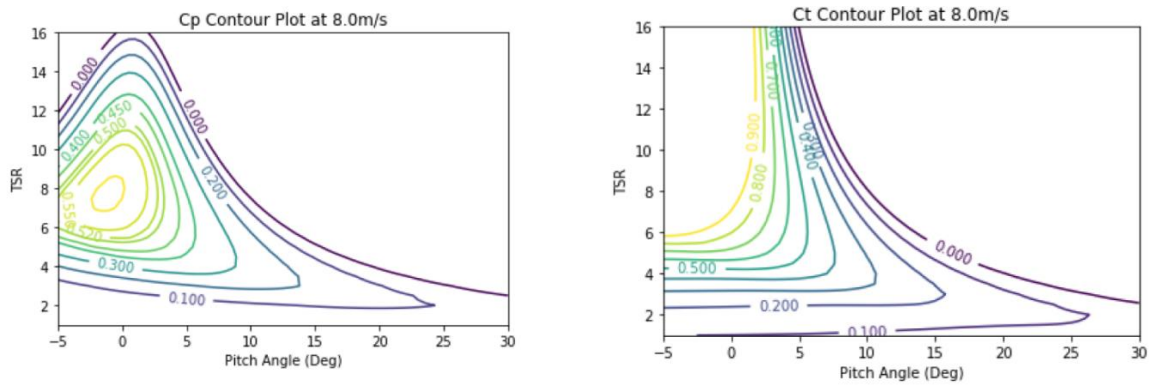

Figure 1. Contour curves of C_p and C_t surfaces.

2.3. The aerodynamic surrogate

In analogy with the flow field computations, computational speed is important for the aerodynamic model when used for optimization purposes. Therefore, a surrogate is developed, which, based on the aerodynamic model described in Section 2.2, mimic the requested data created from this model in a fast and efficient way with sufficient accuracy.

First the steady state performance values of respectively $C_p(U|\alpha,\lambda)$ and $C_t(U|\alpha,\lambda)$ are calculated for every combination of tip speed ratio, pitch angle, and mean wind speed, from a suitable user-defined grid of sample points. Next multi-dimensional polynomial representations of respectively $C_p(U|\alpha,\lambda)$ and $C_t(U|\alpha,\lambda)$ are fitted to the computed grid values, whereby continuous C^1-surfaces are obtained for the surrogates. As the surrogates are to be used in combination with gradient-based optimization algorithms, it is important that the partial derivatives of the constructed continuous multi-dimensional surfaces are continuous. In the present work a spline-interpolation was applied.

2.4. Synthesis and optimization

With modeling of the WPP flow field and the aerodynamic performance of the WPP WT's in place, the next step is to synthesize these in an optimization *objective function*. Without a WPP controller functionality, each individual WT will operate at *maximum* C_p below rated wind speed. The goal for the present optimization process is to find the *optimal balance* between individual WT de-ratings, which result in maximum WPP power production. The optimal WT de-rating settings will clearly depend on the WPP topology and thereby the mean inflow wind direction, θ. It will, moreover, depend on the mean wind speed as long as one or more WT's operates below rated power. Consequently, the optimal WPP operation is formulated as a set control schedules, conditioned on the WPP mean inflow wind speed and the WPP mean inflow wind direction.

The objective function is accordingly defined as

$$P(U,\theta) = \sum_{i=1}^{N} P_i(\lambda_i, \alpha_i | U, \theta) \tag{5}$$

where N denotes the number of WT's in the WPP, and lower indices, i, refer to WT no. i. The optimization problem to be solved is defined in terms of the objective function (5) accompanied by two sets of constraints given by

$$\begin{aligned} \lambda_{min}(U) \le \lambda \le \lambda_{max}(U) \\ \alpha_{p,min} \le \alpha_p \le \alpha_{p,max} \end{aligned} \tag{6}$$

The relevant values for the Siemens SWT-2.3-93 WT used in the example calculations are: $\lambda_{min}(U) = 36\text{ms}^{-1}/U$; $\lambda_{max}(U) = 75.15\text{ms}^{-1}/U$; $\alpha_{p,min} = -2°$; and $\alpha_{p,max} = 90°$.

The workflow in the resulting optimization platform is illustrated in Figure 2. The optimization "module" is based on a re-developed version of TOPFARM [2], [3]. A genetic optimization algorithm (GA) is used for first pass of the solution supplemented by a gradient based method (SLSQP) for final refinement. Finally, it should be noted that for simplicity, it was initially assumed that all rotors are identical and with identical hub heights.

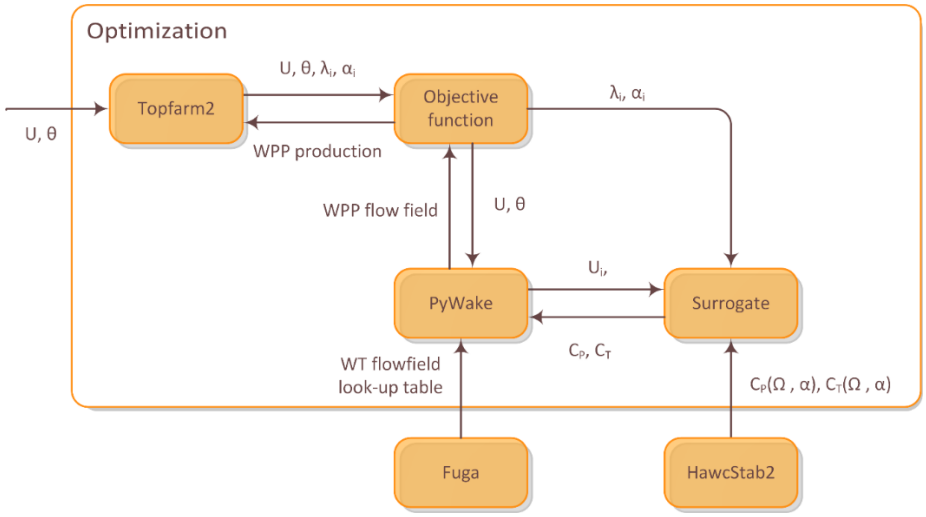

Figure 2. Platform workflow.

3. Sanity check of the platform

The two-parameter workflow presented in Section 2 is tested for its functionality using a simple three-WT case. The WPP layout is shown in Figure 3, where three WT's are placed 300m apart and in a single row. In the sanity check the "no-wake" inflow direction (0 degrees) case will be compared to an inflow case, where wakes are indeed present (90 degrees inflow direction).

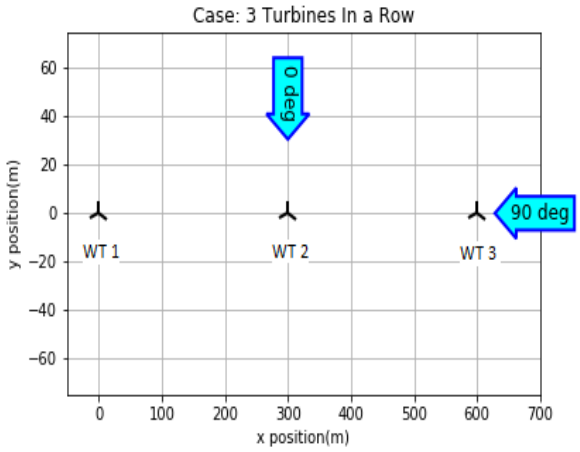

Figure 3. Topology of the three WT test case.

The optimized WPP control schedule for the three WT test case is shown in Figure 4. The WT C_p surface is represented by contour curves in the λ-α plane and, for each of the three WT's, the optimized operation settings are illustrated by the red- and black lines in this plane, respectively. The red line represents optimal settings for the 90-degree inflow case, whereas the black line represents optimal settings for the zero-degree inflow case.

From the optimization results, it is clear that WT de-rating is indeed happening for the 90-case. Firstly, the most downstream turbine (WT1) is operating at "greedy" settings for both tested directions. The middle turbine (WT2) and the most upstream turbine (WT3) are operating at both higher pitch values, and lower tip speed ratio (i.e. rotational speeds) values in the 90-degree case. This shows that both the middle and the most upstream turbines are in fact sacrificing power to increase the available wind resource to the last turbine, who is allowed to operate at its best settings.

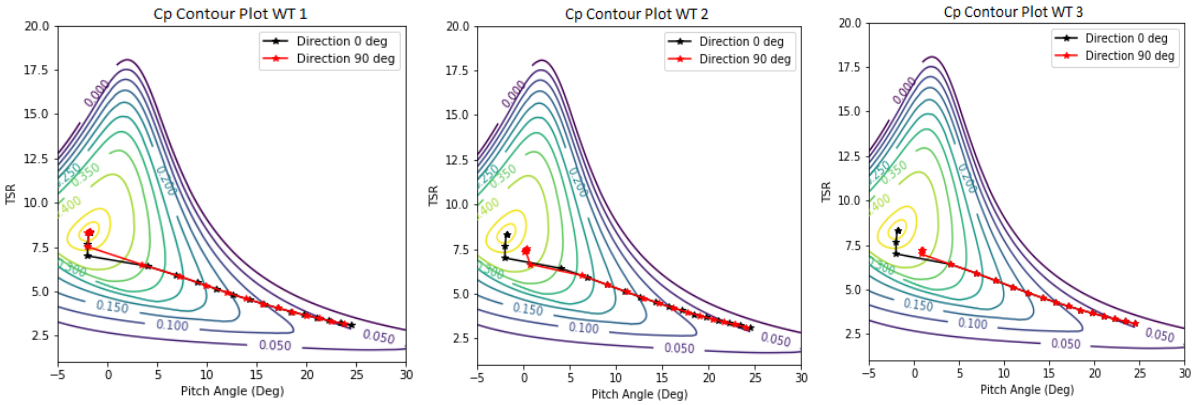

Figure 4. Optimized WPP control schedule for the three WT test case.

Further investigation into the power curves of each WT reveals how production is improved by changing the operational settings. The resulting optimized settings from the two-parameter test (i.e. the λ-α design space) of the 90-degree case are compared to a reference "greedy" power curve, which was obtained by running the optimization tool with only one WT implying that no wake effects are present. This "greedy" curve is imposed on all three of the wind turbines in this row for that exact same direction, wind speed range, and spacing.

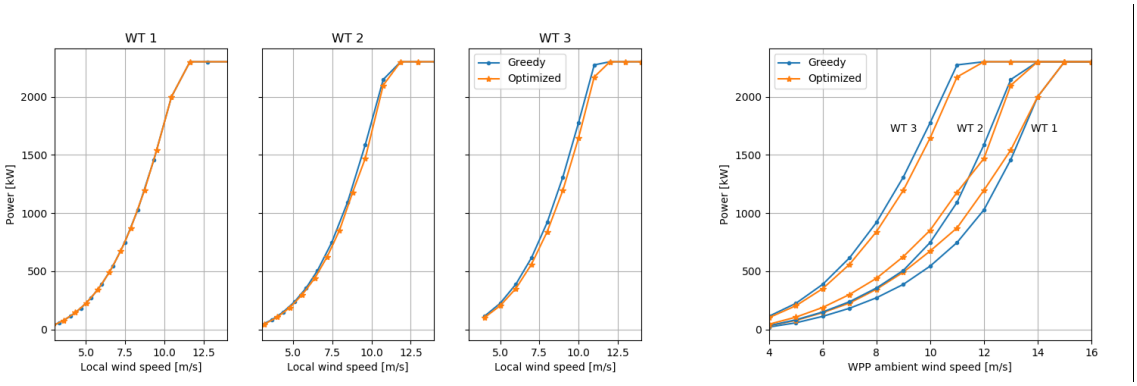

Figure 5. Power for each WT associated with greedy and optimal control settings in the 90-degree case as a function of local (left) and WPP ambient wind speed (right), respectively.

Figure 5 shows the power and the local wind speeds that each turbine is producing/witnessing for each global inflow wind speed tested. Two things are noticeable. Firstly (cf. Figure 5; left), the upstream turbine (WT3) and middle turbine (WT2) have both reduced power curves compared to the "greedy" settings at wind speeds *below rated wind speed*. This implies de-rating is taking place, as shown before. Secondly (cf. Figure 5; right), increased local wind speed, relative to the "greedy" settings case, as well as an increase in the actual power produced are observed for the middle turbine (WT2). Even though this WT is de-rated, the increased *local* wind speed, made possible by de-rating the upstream turbine (WT3), leads to better production compared to the "greedy" settings for the same global inflow wind speed. Furthermore, the most downstream turbine (WT1) benefits even more, as it not only continue to

operate in "greedy" settings but also at a much higher *local* wind speed. This highlights the effect of mitigating wakes and the cubic relationship between power and velocity.

4. Collapse of design space

In this section the conjectured collapse of the design space from two design parameters (i.e. α and λ) to one design parameter representing unique set of (α, λ), representing the lowest thrust coefficient for a given power coefficient, is justified. We will base this investigation on the the 3-WT case study analysed in Section 3, and in particular determine if the optimization tool is implementing one particular strategy below rated wind speed – i.e. the "minimum C_t strategy". Figure 6 shows the α- and λ-values that for given C_p values produce the lowest C_t.

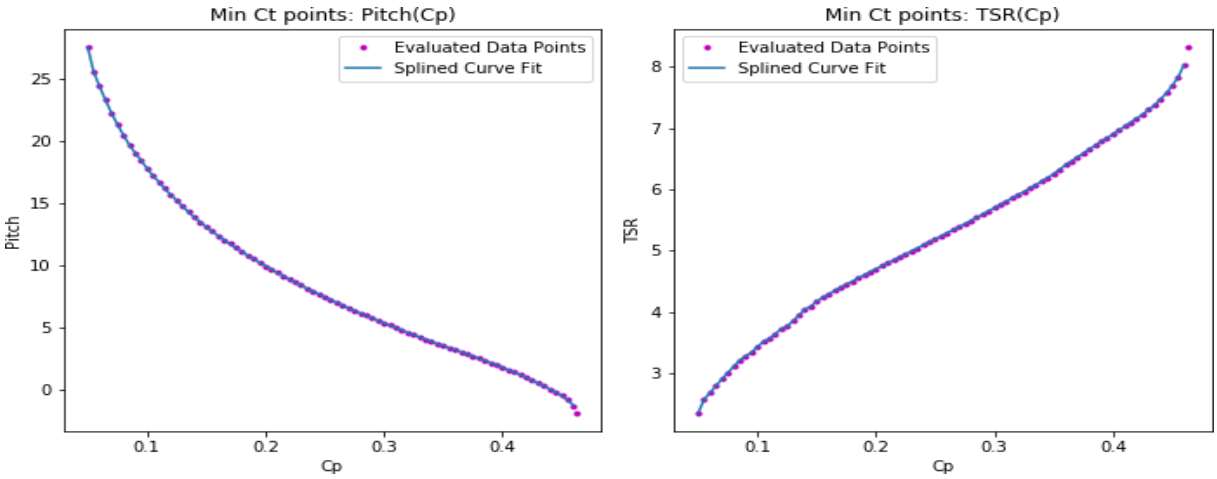

Figure 6. Pitch- and tip speed values, which for given C_p values, produce the lowest WT thrust.

By applying these settings to the middle and upstream turbines of the verification case described in Section 3, it can be seen from Figure 7, that the optimized settings, referring to respectively the two-parameter and one-parameter approach, align very well.

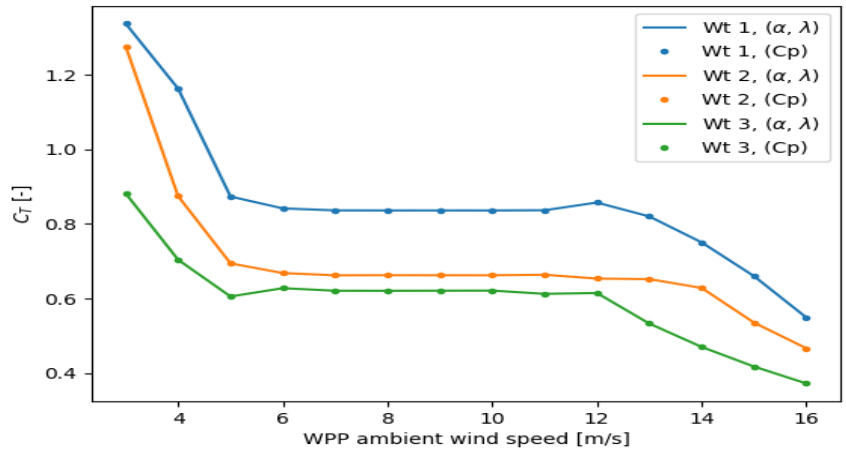

Figure 7. Optimized de-rating settings using respectively one- and two parameter optimization.

This realization made it possible to collapse the design space by implementing the minimum C_t curves onto the workflow of Section 2. Hence, in this way, each individual turbine's operation settings are controlled uniquely through a C_p value. In this constrained design space, the GA solver was no longer needed, as similar results could be obtained using only the gradient based SLSQP solver.

5. The Lillgrund case study - results and discussion

A full-scale WPP control analysis of the offshore Lillgrund WPP is carried out using the one-parameter tool. The Lillgrund WF consists of 48 Siemens SWT-2.3-93 WT's with a layout as shown in Figure 8. The layout of the Lillgrund WPP is characterized by very small WT inter spacing's – i.e. down to 3.3 rotor diameters – and consequently with pronounced wake effects, which makes this WPP ideally suited for WPP control.

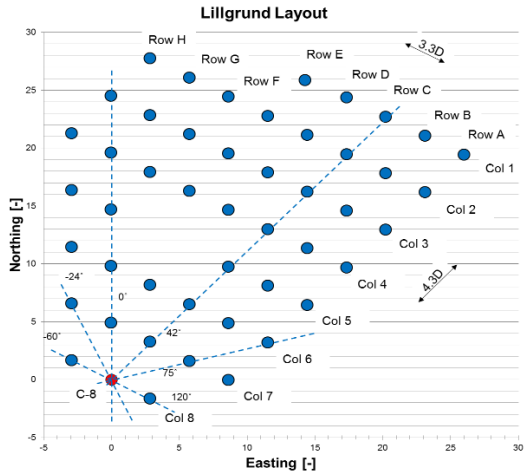

Figure 8. Layout of the Lillgrund WF.

The AEP for the WPP is calculated using the optimized control schedules and compared to the AEP resulting from the traditional "greedy" WT control strategy using site wind characteristics. The complete wind rose is resolved in 30° sectors, and for each of these the sector probability as well as the mean wind speed Weibull parameters (i.e. shape and strength parameter) are given and shown in Table 1.

Table 1: Lillgrund site wind characteristics.

Wind Section (centered)	Wd (%)	Scale (A)	Shape (k)
0 deg	5.4	8.2	1.83
30 deg	4.2	7.6	2.1
60 deg	5.4	8.3	2.29
90 deg	6.6	9.0	2.69
120 deg	8.3	9.8	3.0
150 deg	8.3	9.4	3.16
180 deg	7.6	9.2	2.43
210 deg	10.6	10.1	2.53
240 deg	13.6	10.8	2.81
270 deg	15.4	10.6	2.66
300 deg	9.6	9.4	2.42
330 deg	5.0	9.7	1.92

The WPP energy production is computed for both control strategies conditioned on mean wind speed (1m/s resolution) and mean wind direction (1° resolution), respectively, and subsequently convoluted with mean wind speed distributions and the mean wind direction distribution to obtain the AEP estimate.

An example of a resulting control schedule – conditioned on a mean WPP inflow speed of 10m/s and a mean inflow wind direction of 240° (cf. equation (5)) – is given in Figure 9. For each and every WT, the resulting de-rating percentage is indicated by the WT de-rating colour code. The WPP flow field characteristics are illustrated by the blue wind speed colour code. As seen, optimal de-ratings are, as expected, more pronounced for the upstream WT's affecting the downstream WT's the most, whereas downstream WT's deep into the WPP are either not affected or only affected to a minor extend.

The aggregated AEP results are shown in Figure 10. The left plot of this figure shows the AEP gains *conditioned on the inflow mean wind direction* and with reference to the mean wind speed regime [4m/s;25m/s]. The gain is obviously highly dependent on the inflow direction, with the largest potential gains obtain in cases with massive wake effects as expected. The right plot of Figure 10 shows the AEP gain *conditioned on mean wind speed*. As expected the largest gains are obtained in the WPP mean inflow wind speed regime, where all WT's are operated below rated wind speed. With increasing WPP inflow wind speed, more and more WP's are successively operating above rated wind speed, thus gradually reducing the possible AEP gain.

In total the WPP AEP gain referring to all wind speeds (i.e. 4-25m/s) is approximately 1.0%. If one were only to consider wind speeds between 4m/s to 11m/s, where increased production is possible applying optimized settings, then this gain rises to 1.5%.

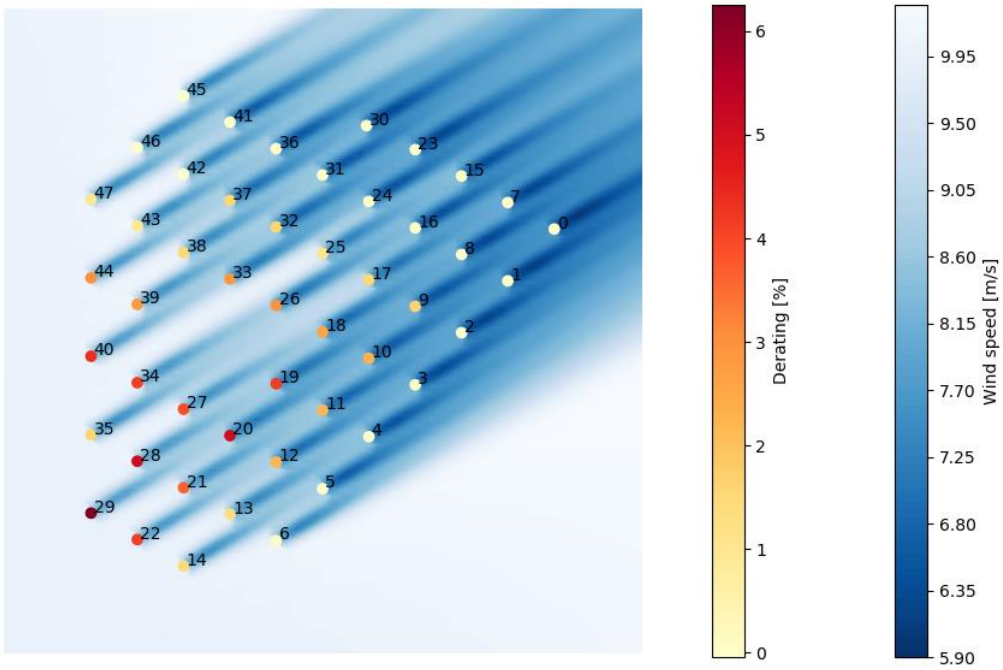

Figure 9. Optimal WT de-ratings associated with mean wind speed 10m/s and wind direction 240°. WPP power gain associated with this specific case is 1.2%.

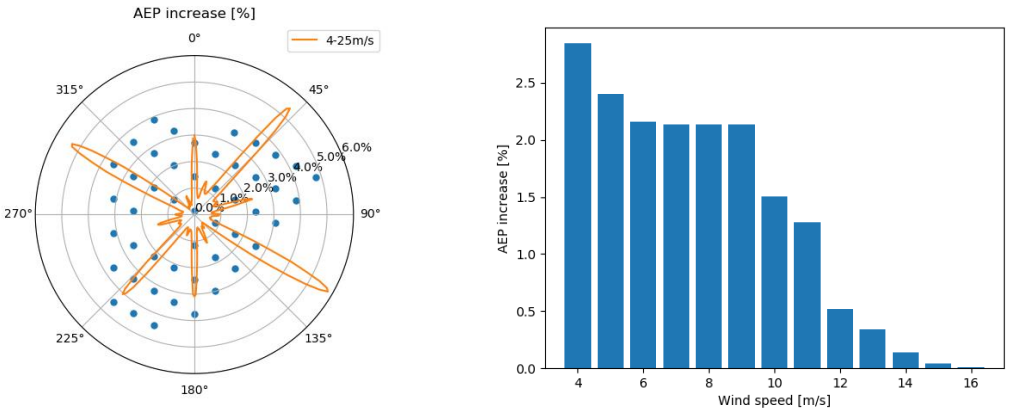

Figure 10. AEP gain obtained using optmized control schedules.

6. Conclusion

A platform for open-loop WPP control optimization has been developed using aggregated WPP production as metric and with a design space spanned by two parameters for each WT - the tip speed ratio and the collective pitch angle.

The functionality of the platform has been "verified" using a simple three WT WPP for simple sanity checks. Using the same simple WPP test case, the validity of collapsing the design space to a space spanned by only one parameter for each WT is justified. The selected parameter reflects the unique combination of tip speed and collective pitch, which, for a given C_p value, results in the minimum C_t value. The fact that the reduced design space is able to produce results identical to the results emerging from the "full" design space makes perfectly sense, since minimum C_t values imply minimum wake effects (i.e. wake deficit as well as wake generated turbulence).

The one-parameter version of the platform is finally used to evaluate the WPP control potential on the existing Lillgrund offshore WPP, and it is demonstrated that production gains are in fact possible through individual de-rating of the WPP WT's. This is encouraging for WPP control scheduling, since the gains can be obtained for virtually no cost compared to the gain they can provide.

WT loading is so far not considered but, given the fact that wake losses to some degree correlate with loading of WPP WT's, it is believed, that the load level in general is not increased as a result of the developed WPP control optimization.

In a future perspective, besides de-rating, active yaw control of WPP WT's should be included. Including active yaw control will definitely emphasize the need to also include load aspects. Finally, as an additional potential benefit, WPP control can ultimately be fully merged into topology optimization of a WPP. This makes sense, since WPP topology optimization depends on WPP control.

Acknowledgements

Financial support from the EU Horizon 2020 research and innovation program, under grant agreement no. 727680 (TotalControl), is acknowledged. Siemens Wind Power is acknowledged for making the aerodynamic data of the Siemens SWT-2.3-93 WT available for the Lillgrund study.

References

[1] S. Ott, J. Berg and M. Nielsen (2011). Linearised CFD Models for Wakes. Risoe-R-1772(EN).

[2] P.-E. Réthoré, P. Fuglsang, G.C. Larsen, T. Buhl, T.J. Larsen, H.Aa. Madsen (2013) TOPFARM: Multi-fidelity optimization of wind farms. Wind Energy, vol. **17**, pp. 1797–1816.

[3] G.C. Larsen, P.-E. Réthoré (2013). TOPFARM – A Tool for Wind Farm Optimization. Energy Procedia, vol. **35**, pp. 317–324.

[4] S. Kanev, W.P. Engels and F. Savenije (2018). Active wake control: An approach to optimize the lifetime operation of wind farms. Wind Energy, vol. **21**, no. 7, pp. 488-501.

[5] J. Lee, B.H. Son and S. Lee (2013). Blade pitch angle control for aerodynamic performance optimization of a wind farm. Renewable Energy, vol. **54**, pp. 124-130.

[6] J.S. González, M.B. Payán, J.R. Santos and Á.G.G. Rodríguez (2015). Maximizing the overall production of wind farms by setting the individual operating point of wind turbines. Renewable Energy, vol. **80**, pp. 219-229.

[7] G.C. Larsen, T.J. Larsen, S. Ott, K.S. Hansen and H.Aa. Madsen (2012). Full Scale Verification of Wind Farm Production Predictions. XXIII ICTAM, 19-24 August 2012, Beijing, China.

[8] G.C. Larsen, H.Aa, Madsen, K. Thomsen and T.J. Larsen (2008). Wake meandering - a pragmatic approach. Wind Energy, **11**, pp. 377–395.

[9] T.J. Larsen, H.Aa. Madsen, G.C. Larsen and K.S. Hansen (2013). Verification of the Dynamic Wake Meander Model for Loads and Power Production in the Egmond aan Zee Wind Farm. Wind Energy, **16**, pp. 605–624.

[10] H.Aa. Madsen, G.C. Larsen, T.J. Larsen, N. Troldborg (2010). Calibration and validation of the dynamic wake meandering model for implementation in an aeroelastic code. Journal of Solar

Energy Engineering 2010; **132**(4): 041014 (14 pages).

[11] Pywake URL https://gitlab.windenergy.dtu.dk/TOPFARM/PyWake.

[12] M.H. Hansen, L.C. Henriksen, C. Tibaldi, L. Bergami, D. Verelst and G. Pirrung (2017). HAWCStab2 User Manual. DTU Wind Energy.

[13] H.Aa. Madsen, R. Mikkelsen, N.N. Sørensen, M.L.O. Hansen, S. Øye and J. Johansen (2007). Influence of wind shear on rotor aerodynamics, power and loads. Research in Aeroelasticity EFP-2006, Risø-R-1611(EN).